Accepted Manuscript

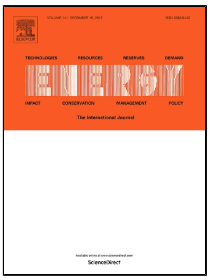

Computational fluid dynamic simulation of a sorption-enhanced palladium membrane reactor for enhancing hydrogen production from methane steam reforming

Guozhao Ji, Ming Zhao, Geoff Wang

PII:	S0360-5442(18)30110-5
DOI:	10.1016/j.energy.2018.01.092
Reference:	EGY 12204
To appear in:	*Energy*
Received Date:	18 February 2017
Revised Date:	22 November 2017
Accepted Date:	18 January 2018

Please cite this article as: Guozhao Ji, Ming Zhao, Geoff Wang, Computational fluid dynamic simulation of a sorption-enhanced palladium membrane reactor for enhancing hydrogen production from methane steam reforming, *Energy* (2018), doi: 10.1016/j.energy.2018.01.092

Computational fluid dynamic simulation of a sorption-enhanced palladium membrane reactor for enhancing hydrogen production from methane steam reforming

Guozhao Ji [a], Ming Zhao [a,*] and Geoff Wang [b]

[a] School of Environment, Tsinghua University, Beijing 100084, China

[b] School of Chemical Engineering, the University of Queensland, Brisbane, Qld 4072, Australia

* Corresponding Author. Tel: +86 10 62784701. Email: ming.zhao@tsinghua.edu.cn

Abstract

To understand the reaction process of methane steam reforming in a sorption enhanced membrane reactor (SEMR), a computational fluid dynamic (CFD) model was developed to simulate the methane (CH_4) steam reforming in a palladium-based membrane reactor using a Ni-based catalyst and Na_2ZrO_3 CO_2 sorbent. The CFD model gained the insight of details in the reactor which could not be obtained by experiment. With the detailed information, this model detected the difference of reaction kinetics and fluid dynamic conditions in a SEMR and a traditional membrane reactor (MR). The comparison suggests that sorption-enhanced membrane reactor not only decreases CO_2 fraction, but also improves hydrogen (H_2) production by increasing reaction rates, CH_4 conversion and H_2 yield. The poisoning effect of carbon monoxide (CO) on the palladium membrane can also be minimized by reduced CO

fraction as a result of *in-situ* CO_2 capture.

Keywords: CFD simulation; sorption-enhanced membrane reactor; methane steam reforming; hydrogen production; Ni catalyst; Na_2ZrO_3 sorbent

1. Introduction

Currently, fossil fuels are still the primary source for satisfying the growing energy demand of our contemporary society. However, the growing level of CO_2 from the emission of fossil fuel combustion is increasing the concern of global warming. In the case of low carbon emission technologies, H_2 becomes an attractive alternative, mainly due to its high calorific value and non-polluting emission [1]. H_2 can be produced via thermo-chemical processes from a variety of sources including biomass [2, 3], natural gas [4, 5], coal [6, 7], water [8, 9], and some industrial waste chemicals [10]. For most of these H_2 production technologies, methane steam reforming (MSR), referring to Eqn. R1 below, is a necessary step to convert CH_4 and water to H_2 [11].

$$CH_4 + H_2O \rightleftharpoons CO + 3\ H_2 \qquad \Delta H_{298}=-206.1\ \text{kJ mol}^{-1} \qquad \text{(R1)}$$

However the H_2 yield through reaction (R1) is accompanied with approximately 25 vol.% toxic gas CO. To avoid producing the toxic gas, water-gas shift (WGS) reaction is usually implemented to further convert CO into H_2 and a by-product CO_2 (Eqn. R2).

$$CO + H_2O \rightleftharpoons CO_2 + H_2 \qquad \Delta H_{298}=41.15\ \text{kJ mol}^{-1} \qquad \text{(R2)}$$

It should be noted that reaction (R1) is endothermic and reaction (R2) is exothermic, which prevents them achieving high conversion simultaneously in a single reactor where they are in the same temperature range. It is generally required to control MSR at temperatures higher than 700 ºC. However WGS reacts efficiently only below 450 ºC. For ordinary MSR hydrogen production, the hot gas mixture has to be delivered from MSR reactor to WGS reactor, which resulted in a large energy penalty due to the cooling down between reactors. In order to minimize this impact, a membrane reactor was invented to allow these two reactions to proceed simultaneously in a single reactor with better CH_4 conversion and improved H_2 production. The membrane is designed to be H_2 selective, thus that H_2 could be partially removed continuously from the reactor by membrane permeation, meanwhile sustaining other gas components in the reactor. In turn, the equilibriums of MSR and WGS are shifted towards the H_2 side owing to the H_2 removal. Therefore, separating H_2 at high temperatures becomes attractive due to the reduction of energy penalties associated with the cooling encountered in traditional MSR.

Among potential gas separation technologies, inorganic membranes such as palladium-based membranes [12, 13] and silica-based membranes [14, 15] have performed well at high temperatures. These membranes have been deployed in membrane reactor configurations for H_2 production via MSR [16, 17], WGS reactions [18, 19], as well as dehydrogenation reactions [20]. The CH_4 conversion enhancement mainly depends on the H_2 permeation. As is known that increasing the sweep flow could improve H_2 permeation. Anzelmo et al. enhanced the CH_4 conversion from

about 50% to 84% by varying the sweep flow 0 to 100 ml min^{-1} [21].

Based on open literatures in membrane reactor design, palladium-based membranes showed superior popularity over silica-based membranes for its infinite H_2 selectivity and higher permeability [22, 23], though its capital cost is 2 orders of magnitudes higher than the silica counterpart. However, CO, which is an inevitable gas component in MSR, is an inhibitor for the palladium membrane because it affects the H_2 dissociation path [24]. The presence of CO is attributed to the faster reaction of MSR than that of WGS. The net gain of CO accumulates in the reactor. Enhancing the CO conversion is a feasible solution to reduce the CO concentration and resultantly minimize its inhibition effect to palladium. Sufficiently removing H_2 could possibly achieve this goal in some situations. But once the membrane reactor needs to process large quantity of gases, the high space velocity doesn't give sufficient retention time for reactants to react and for H_2 to permeate. Membrane reactors still suffer from low conversions with high space velocities [25, 26].

Apart from H_2 removal by membrane, capturing the other product gas (CO_2), may further shift the WGS reaction equilibrium towards H_2+CO_2 side and in turn enhance the CO conversion. Furthermore, the CO depletion resulted from CO_2 capture would also enhance the MSR reaction towards the H_2 side because CO is one of the products of MSR. Regarding the *in-situ* CO_2 capture, various materials such as CaO, Na_2ZrO_3, and hydrotalcite have been used as sorbents and some of them was successfully deployed to enhance MSR [27-31] and WGS [32]. If these sorbent materials were integrated with membrane separation, a further enhancement of 'shift effect' could be

expected for MSR. This type of configuration is called sorption enhanced membrane reactor (SEMR). However, the number of publications with this idea is very limited [33, 34]. Only Li et al. [33] and Madeira et al. [34] had used hydrotalcite as CO_2 sorbent in palladium membrane for WGS. Other sorbent materials could also be applied in membrane reactors for MSR. The limited number of studies using both membrane and sorbents was owing to the complexity of synergistic effects among MSR, WGS, membrane permeation and CO_2 capture. Moreover, these synergistic effects were difficult to be studied experimentally. Zhang et al.[35] and Chen et al.[36] deployed one dimensional 'plug flow' model to calculate the sorption enhanced membrane reactor performance. However, plug flow model was criticized by Koukou et al.[37] due to the inadequacy in considering radial profile. CFD simulation which gives the distributed three-dimensional information is need to get an insight of reaction details in a reactor. There hasn't been a CFD model study to interpret and analyze the MSR performance in a SEMR. This study for the first time will deploy CFD simulation to fill this knowledge gap and fulfill the need of investigating the coupled processes and assist the analysis of the shift effect.

This work is aimed to investigate the enhancement of MSR process by applying membrane separation and *in-situ* CO_2 sorption together in one reactor as described in Fig. 1. The processes in this reactor include MSR, WGS, H_2 permeation and CO_2 sorption. H_2 permeation and CO_2 capture reduce the product concentration and shift the reactions towards products side on basis of Le Chatelier's principle. The dynamics and the equilibria of these processes depend on the fluid dynamic conditions such as

gas component concentration, pressure and temperature. In turn, these processes will also affect the fluid dynamic conditions. All the processes and fluid dynamic conditions are inter-correlated and spatially distributed in a reactor. It is extremely difficult, if not impossible, to measure all the concerned parameters inside the reactor experimentally. In order to better understand the reaction processes, detailed information (e.g. gas concentration distribution) inside a reactor should be studied. To address this problem, computational fluid dynamics (CFD) simulation can be used to correlate fluid dynamics with space coordinate and time [38], thus provide detailed gas flow characteristics and the distributed reaction kinetics in a membrane reactor with CO_2 sorption for MSR. The source term in CFD allowed the reactions and permeation to be written in the CFD governing equations to couple the microscopic model (reactions, permeation) with macroscopic model (fluid dynamics). As a result, the CFD simulation can become a feasible tool to improve the design of given membrane reactor and improve the operation of methane steam reforming in the membrane reactor. Therefore, we will carry out a CFD simulation of SEMR. The simulation with distributed information such as reaction rates and gas concentrations would assist the analysis and improvement of the reactor performance, especially the CH_4 conversion and CO concentration.

2. Model description

The design of the membrane reactor investigated in this work is depicted in Fig. 2.

The reactant gases, CH_4+H_2O, were fed from the inlet of the reactor. As the gases flowed in the catalyst packed bed, MSR and WGS proceeded. The generated H_2 that permeated across the membrane was collected with sweep N_2 via the outlet. The unpermeated gas exited the reactor from the right outlet. For the case with *in-situ* CO_2 sorption, the catalyst would mix with CO_2 sorbents and some generated CO_2 may be captured by the sorbents.

The MSR, WGS, H_2 permeation and CO_2 sorption only occur between the feed inlet and the outlet of the unpermeated gas. For simplicity, the CFD model only simulated the processes in the zone between the membrane and the reactor shell, which is made from a hollow cylinder. In view of the axial symmetry of the reactor, a 15º portion of the reacting zone with symmetry planes on both side was simulated to save the computational time (Fig. 3). The boundary condition of inlet was mass flowrate with fixed composition of CH_4 and H_2O vapor. The outlet was a pressure opening. The reactor shell was set as wall. The membrane was also set as wall, but with negative H_2 mass source to represent the H_2 permeation. At the two symmetries, there was no tangential gradient for any variables. The structured mesh was created from inlet to outlet by sweep method to facilitate the computation speed.

The CFD model is mathematically expressed by the governing equations consisting of continuity equations and momentum equations. The continuity equation governs the mass balance, giving

$$\frac{\partial c}{\partial t}+\frac{1}{r}\frac{\partial}{\partial r}\left(r\cdot c\cdot u_r\right)+\frac{1}{r}\frac{\partial}{\partial \theta}\left(c\cdot u_\theta\right)+\frac{\partial}{\partial z}\left(c\cdot u_z\right)=S_{\mathrm{ct}} \quad (1)$$

where S_{ct} is the source term caused by the processes which break the total mass

balance such as H_2 permeation and CO_2 sorption. The momentum balance can be expressed by the Navier-Stokes equation as follows

$$\frac{\partial u_r}{\partial t}+u_r\frac{\partial u_r}{\partial r}+\frac{u_\theta}{r}\frac{\partial u_r}{\partial \theta}-\frac{u_\theta^2}{r}+u_z\frac{\partial u_r}{\partial z} =-\frac{1}{\rho}\frac{\partial p}{\partial r}+\frac{\eta}{\rho}\left[\frac{1}{r}\frac{\partial}{\partial r}\left(r\frac{\partial u_r}{\partial r}\right)+\frac{1}{r^2}\frac{\partial^2 u_r}{\partial \theta^2}+\frac{\partial^2 u_r}{\partial z^2}-\frac{u_r}{r^2}-\frac{2}{r^2}\frac{\partial u_\theta}{\partial \theta}\right]-S_{\mathrm{r}} \tag{2}$$

$$\frac{\partial u_\theta}{\partial t}+u_r\frac{\partial u_\theta}{\partial r}+\frac{u_\theta}{r}\frac{\partial u_\theta}{\partial \theta}-\frac{u_r u_\theta}{r}+u_z\frac{\partial u_\theta}{\partial z} =-\frac{1}{\rho}\frac{\partial p}{\partial \theta}+\frac{\eta}{\rho}\left[\frac{1}{r}\frac{\partial}{\partial r}\left(r\frac{\partial u_\theta}{\partial r}\right)+\frac{1}{r^2}\frac{\partial^2 u_\theta}{\partial \theta^2}+\frac{\partial^2 u_\theta}{\partial z^2}-\frac{u_\theta}{r^2}-\frac{2}{r^2}\frac{\partial u_r}{\partial \theta}\right]-S_\theta \tag{3}$$

$$\frac{\partial u_z}{\partial t}+u_r\frac{\partial u_z}{\partial r}+\frac{u_\theta}{r}\frac{\partial u_z}{\partial \theta}+u_z\frac{\partial u_z}{\partial z} =-\frac{1}{\rho}\frac{\partial p}{\partial z}+\frac{\eta}{\rho}\left[\frac{1}{r}\frac{\partial}{\partial r}\left(r\frac{\partial u_z}{\partial r}\right)+\frac{1}{r^2}\frac{\partial^2 u_z}{\partial \theta^2}+\frac{\partial^2 u_z}{\partial z^2}\right]-S_{\mathrm{z}} \tag{4}$$

where S_{r}, S_θ and S_{z} represent the momentum source (or momentum loss) in radial and axial direction caused by the packed catalyst and sorbent.

Further for a multi-component system, the continuity equation of each component is described as

$$\frac{\partial c_i}{\partial t}+\frac{1}{r}\frac{\partial}{\partial r}\left(r\cdot c_i\cdot u_r\right)+\frac{1}{r}\frac{\partial}{\partial \theta}\left(c_i\cdot u_\theta\right)+\frac{\partial}{\partial z}\left(c_i\cdot u_z\right) =\frac{1}{r}\frac{\partial}{\partial r}\left(r\cdot D\frac{\partial c_i}{\partial r}\right)+\frac{1}{r}\frac{\partial}{\partial \theta}\left(D\frac{\partial c_i}{\partial \theta}\right)+\frac{\partial}{\partial z}\left(D\frac{\partial c_i}{\partial z}\right)+S_i \tag{5}$$

where S_i is the source term of each component which is depleted or generated by chemical reactions as well as selective permeation. In this study for methane steam reforming, i=CH_4, CO_2, CO, H_2, H_2O.

Apart from reactions (R1) and (R2), there are some other possible reactions together with MSR listed as follows

$$CH_4 + 2\ H_2O \rightleftharpoons CO_2 + 4\ H_2 \qquad \Delta H_{298}\text{=-165.0 kJ mol}^{-1} \tag{R3}$$

$$CH_4 + CO_2 \rightleftharpoons 2\ CO + 2\ H_2 \qquad \Delta H_{298}\text{=-247.3 kJ mol}^{-1} \tag{R4}$$

$$CH_4 + 3\ CO_2 \rightleftharpoons 4\ CO + 2\ H_2O \qquad \Delta H_{298}\text{=-330.0 kJ mol}^{-1} \tag{R5}$$

Reaction (R3) can be considered as a superposition of (R1) and (R2). However, it has been proved that (R4) and (R5) don't occur in methane steam reforming [39, 40]. Thus these two reactions were not taken account in this model.

Ni-based catalyst was the most widely utilized catalyst in palladium MSR reactors due to the low cost and high CH_4 conversion [41]. The MSR reaction rate under the catalysis (Ni/Al_2O_3) was assumed to follow Langmuir-Hinshelwood-Hougen-Watson (LHHW) model [40, 42]

$$r_{\mathrm{MSR}} = \frac{k_{\mathrm{MSR}}}{p_{\mathrm{H_2}}^{2.5}} \frac{\left(p_{\mathrm{CH_4}} p_{\mathrm{H_2O}} - \dfrac{p_{\mathrm{H_2}}^3 p_{\mathrm{CO}}}{K_{\mathrm{MSR}}} \right)}{DEN^2} \tag{6}$$

where K_{MSR} is the equilibrium constant for MSR. k_{MSR} is the rate coefficient of MSR. These values are functions of temperature and generally follow the Arrhenius correlation, giving

$$k_{\mathrm{MSR}} = k_{\mathrm{MSR,r}} \exp\left[-\frac{E_{\mathrm{k,MSR}}}{\mathrm{R}T} \right] \tag{7}$$

$$K_{\mathrm{MSR}} = K_{\mathrm{MSR,r}} \exp\left[-\frac{E_{\mathrm{K,MSR}}}{\mathrm{R}T} \right] \tag{8}$$

where $E_{\mathrm{k,MSR}}$ and $E_{\mathrm{K,MSR}}$ are the activation energies for rate coefficient and

equilibrium constant, respectively, R is the gas constant and T is absolute temperature.

The term in the bracket $\left(p_{CH_4} p_{H_2O} - \frac{p_{H_2}^3 p_{CO}}{K_{MSR}} \right)$ can be seen as the reaction driving force. When all the gas compositions reach equilibrium, this term equals zero. H_2 removal or CO depletion would break the equilibrium and increase the value of this term, thus increase the reaction rate.

Similarly, for WGS reaction, the rate is

$$r_{WGS} = \frac{k_{WGS}}{p_{H_2}} \frac{\left(p_{CO} p_{H_2O} - \frac{p_{H_2} p_{CO_2}}{K_{WGS}} \right)}{DEN^2} \tag{9}$$

The rate coefficient and equilibrium constant of WGS are

$$k_{WGS} = k_{WGS,r} \exp\left[-\frac{E_{k,WGS}}{RT} \right] \tag{10}$$

$$K_{WGS} = K_{WGS,r} \exp\left[-\frac{E_{K,WGS}}{RT} \right] \tag{11}$$

Since MSR is endothermic, $E_{k,MSR}$ is positive and K_{MSR} increases with temperature. But E_{WGS} is negative due to the exothermic characteristic of WGS reaction. The reaction driving force term $\left(p_{CO} p_{H_2O} - \frac{p_{H_2} p_{CO_2}}{K_{WGS}} \right)$ mathematically implied the removal of both H_2 and CO_2 from the reactor would result in a higher driving force than the case with removal of either of them.

The adsorption factor in Eqns. (6) and (9) is defined as

$$DEN = 1 + K_{CO} p_{CO} + K_{H_2} p_{H_2} + K_{CH_4} p_{CH_4} + K_{H_2O} \frac{p_{H_2O}}{p_{H_2}} \tag{12}$$

Eqns. (6) and (9) reflect the mechanism of the reaction enhancement by H_2 permeation. In the case of membrane reactor, H_2 partial pressure (p_{H_2}) decreases when the H_2 permeation occurs. Reaction rates of MSR (r_{MSR}) and WGS (r_{WGS}) increase by decreasing H_2 partial pressure (p_{H_2}). Eqn. (9) also indicates that lowering CO_2 partial pressure (p_{CO_2}) could directly favor the WGS (r_{WGS}). WGS reduces CO partial pressure (p_{CO}), then MSR is enhanced in the meantime.

The H_2 permeation across palladium membrane has been well modeled by Sieverts law [41, 43, 44]

$$J_{H_2} = Q\frac{dp_{H_2}^{0.5}}{dl} \tag{13}$$

where J_{H_2} is the H_2 permeation flux across palladium membrane and Q is the H_2 permeability. l is the coordinate in the membrane thickness direction.

Na_2ZrO_3, which showed decent CO_2 capacity (volume based), fast sorption kinetic and excellent cyclic stability [45-51], could be mixed with Ni/Al_2O_3 catalyst as the sorbent for *in-situ* CO_2 sorption. To obtain CO_2 sorption kinetics data, a TGA (Thermo-gravimetric analysis) test was carried out using Na_2ZrO_3 powder at 500 ºC under various CO_2 partial pressures (0.1, 0.3, 0.5 and 0.7 bar). The measured CO_2 uptakes shown in Fig. 4 suggested that the sorption kinetic is a function of sorbent conversion and CO_2 partial pressure. A polynomial fitting was applied to develop a correlation between the sorption kinetics with sorbent conversion and CO_2 partial pressure. The sorption rate is expressed as

$$r_{CO_2} = \rho_{mol} M_{max} \frac{d\alpha}{dt} \quad (14)$$

where ρ_{mol} is the apparent molar density of the sorbent and M_{max} is the maximum CO_2 molar capacity. The fitted correlation from the experimental sorption test was included in the CFD model to account for CO_2 depletion in the reactor.

The sorbent conversion is a function to time based on Eqn. (15), giving

$$\alpha_{t+\Delta t} = \alpha_t + \frac{d\alpha}{dt} \Delta t \quad (15)$$

In addition to CO_2 capture, Na_2ZrO_3 was also reported for some catalytic effect in reforming and WGS reactions [52]. However, the catalytic effect from alkali catalyst occurs only when the temperature is greater than 800 ºC [53], thus this model assumed that the catalytic effect of Na_2ZrO_3 is minor compared to that of Ni and the catalytic effect of Na_2ZrO_3 was not taken into account in the model.

3. Mesh and time-step independence study

The flow diagram for the entire CFD model was illustrated in Fig. 5. The model was solved by the commercial CFD code CFX (ANSYS Inc., US) in double precision mode.

The partial differential equations (PDE) from (1) to (5) are continuous in space and time. However, discretization must be adopted by mesh size and time step whereby

241 the equations are replaced by the approximations using finite element method.
242 Numerical error is inevitable in finite element method, especially when the mesh size
243 and time step are large. Smaller mesh size and time step can deliver more precise
244 result but prolong the computational time. To ensure the precision of results from this
245 model, mesh and time-step independence study was performed by gradually reducing
246 mesh and time-step from a larger value until the results didn't change with mesh and
247 time-step.

248 Under several mesh sizes and time-steps, the CH_4 mass fraction at a point which
249 locates 1 cm from the inlet was recorded with simulation time. The reason to select
250 this monitoring point is that reactants are rich in this region and reactions are more
251 severe. It is more sensitive to detect the difference of result from different mesh
252 system. Meanwhile this point would give a quick response to the inlet flow to save the
253 simulation time. As shown in Fig. 6, the comparison of different time-step Δt showed
254 that reducing Δt from 0.001 s to 0.0005 s present no difference in the result,
255 suggesting that Δt has little effect on the precision of results. As such, the Δt=0.001 s
256 was used throughout this work. When the minimum mesh size was reduced from 2
257 mm to 0.5 mm, the monitored results were different, which implied that 2 mm mesh
258 size is too rough in this situation. Reducing the mesh size further to 0.3 and 0.1 mm
259 delivered same results to 0.5 mm mesh, which means 0.5 mm mesh size is already
260 sufficiently small to be used in approximating the PDE equations of the CFD model.
261 Finally the mesh system used in this study is 5632 hexahedra (number of nodes: 7965)
262 with max edge length ratio of 1.4634 and volume of 5.19955×10^{-7} m^3.

4. Model validation and results

To validate this model, the model geometry and boundary conditions were set the same as the experiment reported by Tong et al. [54] who carried out comprehensive tests by using different palladium membrane reactors (Membrane_L and Membrane_H) to produce H_2 from MSR with varied space velocities (1120, 2240 and 3360 h^{-1}). The reactor configuration was demonstrated in Fig. 2 and the detailed boundary conditions were listed in Table 1. The experiment was conducted in a membrane reactor without *in-situ* CO_2 capture. So in the first step, the CFD model for membrane reactor (MR) only included MSR, WGS and H_2 permeation, but CO_2 sorption was not considered in this model. The results from this model was denoted as MR. This model was run for validation purpose. In the second step, it is assumed 20% volume were occupied by Na_2ZrO_3 sorbent, thus the *in-situ* CO_2 sorption was included in the CFD model for sorption enhanced membrane reactor (SEMR). The results from the model taking account of the CO_2 sorption was denoted as SEMR. The convergence criteria for all the simulations was set as 1×10^{-5} which means all the errors of continuity equation, and each component (CH_4, CO_2, H_2, CO, H_2O) continuity equation have to be less than 1×10^{-5}.

CH_4 conversion measured by experiment and computed from the CFD model under identical operating conditions were compared for model validation (Fig. 7**)** for two membrane reactors. It can be seen that the simulated CH_4 conversion shown in

Fig. 7 fits very well with the experimental CH_4 conversion reported by Tong et al.[54]. Based on this good agreement, this model is considered accurate permitting its utilization for further simulations into understanding and analysis of the processes in the reactor.

The further comparison was made between MR model and SEMR model (Fig. 8). The addition of CO_2 sorbents in SEMR model dramatically promoted the CH_4 conversion with the greatest enhancement of 37% for 3360 h^{-1} space velocity. For the case of 3360 h^{-1}, the advantage of SEMR over MR prevailed from around the 1st sec until 300th sec. Prior to the 1st sec, the CO_2 sorption hadn't commenced yet. This is because the sorption rate is slow when the sorbent conversion α is low (Fig. 4). Therefore, during this initial period, the SEMR showed little difference from MR. Once the sorbents started to capture CO_2 efficiently, CH_4 conversion increased due to the equilibrium shifting caused by CO_2 sorption. As the sorbent conversion approached to saturation ($\alpha \rightarrow 1$) when the sorbents were used for longer time, the CO_2 sorption kinetic decreased to almost zero as presented in Fig. 4. Thus the MSR and WGS enhancement by sorption would vanish. Therefore, the CH_4 conversion in SEMR dropped to the level of that in MR.

In order to reveal the reason of the different performance in MR and SEMR, the map of CO_2 molar fractions on the symmetry plane (refer to Fig. 3) at the 100th sec in MR and SEMR were compared in Fig. 9. In the MR, CO_2 fraction was increasing with the flow (from inlet to outlet) due to the accumulation of generated CO_2 from WGS reaction. In the radial direction (from membrane to reactor shell), CO_2 fraction

306 slightly decreased. This is because the H_2 permeation promoted WGS, thus WGS
307 produced more CO_2 at the vicinity of the membrane. On the contrary, in the sorption
308 enhanced membrane reactor, CO_2 fraction decreased with the flow, which indicated
309 that the CO_2 sorption rate is close to the CO_2 generation rate from WGS. The level of
310 CO_2 fraction is 2 orders of magnitudes lower in the SEMR than in the simple MR.

311 Since WGS reaction could be enhanced directly by the *in-situ* CO_2 sorption, the
312 map of WGS reaction rate (r_{WGS}) in each reactor was then graphed in Fig. 10. In MR,
313 the WGS reaction rate decreased in the radial direction (from membrane surface to the
314 reactor shell), confirming the enhancement by H_2 permeation as the effect was greater
315 near the membrane. The decrement of WGS reaction rate in the axial direction from
316 the inlet to the outlet is due to the CO_2 fraction increment, which reduced the WGS
317 driving force based on Eqn. (9). Since the overall CO_2 fraction in SEMR is much
318 lower than that MR, around 1 order of magnitude higher reaction rate was observed
319 for the SEMR owing to the CO_2 sorption.

320 As mentioned above for palladium-based membrane, the presence of CO inhibits
321 H_2 dissociation and permeation, so the CO concentration level in a palladium
322 membrane reactor is of special importance. Fig. 11 showed the CO molar fraction
323 distribution in the two reactors. Significant reduction of CO fraction was seen in
324 SEMR, which is below 0.2% throughout the entire membrane length. But in the
325 simple MR reactor, the CO fraction reached up to 1.3%. Consequently, the palladium
326 membrane suffers a higher risk of performance decay.

327 With higher WGS reaction rates, according to Eqn. (6) the rate of methane steam

328 reforming would be further enhanced as a consequence of lower CO fraction. This
329 prediction was confirmed by the methane steam reforming rate (r_{MSR}) in Fig. 12,
330 which showed that SEMR reformed methane at a faster rate than MR. If the methane
331 steam reforming rate at any location in SEMR is faster than that in MR, the overall
332 CH_4 converted must be more for SEMR. This map of methane steam reforming rate
333 (Fig. 12) explained why SEMR improved CH_4 conversion by 37% (Fig. 8).

334 The main target of the whole process is to produce H_2, therefore, H_2 production is
335 of the greatest interest in methane steam reforming. On basis of reactions (R1) and
336 (R2), H_2 yield is directly related to the MSR and WGS rate. Figs. 12 and 10 had
337 demonstrated the improvement of MSR and WGS for SEMR, thus higher H_2 fraction
338 could be certainly expected from SEMR. Fig. 13 displayed the H_2 fraction map of MR
339 and SEMR. The comparison demonstrated evident enhancement of H_2 concentration
340 in SEMR. The generated H_2 would eventually be collected in the permeate stream as
341 pure H_2 and the outlet stream as H_2 rich gas. The remarkable enrichment of H_2 in the
342 reactor would provide a higher driving force for the membrane permeation. The
343 calculated H_2 permeation of SEMR being 2.87×10^{-4} mol s^{-1} was 29% higher than that
344 of MR being 2.23×10^{-4} mol s^{-1}. In addition to the pure H_2 production in the permeate
345 stream, the unpermeated H_2 was also collected in the meantime at the outlet stream.
346 The H_2 flow at the outlet was 8.42×10^{-5} mol s^{-1} for SEMR and 5.67×10^{-5} mol s^{-1} for
347 MR. H_2 dry base fraction at the outlet was 80.79 mol.% for SEMR and 34.47 mol.%
348 for MR. Beside the pure H_2 in permeate stream, the SEMR configuration can also
349 produce high purity H_2 in the outlet stream owing to the decline of CO, CO_2 (Fig. S1)

and more complete conversion of CH_4.

The variations of CO_2 fraction, WGS rate, CO fraction, MSR rate and H_2 fraction are plotted as curves along a line from inlet to outlet in Fig. 14. The location of the line to extract those values is shown in Fig. 14(a). The reductions of outlet CO_2 and CO were more than 95% by deploying SEMR. The reduced CO_2 and CO concentration in the SEMR almost doubled the WGS rate and MSR rate, which made the reactor rich in H_2. The SEMR showed superior performance over simple MR in terms of CH_4 conversion, CO reduction and H_2 yield.

Sensitivity analysis of operating parameters in this SEMR CFD model is a pathway to identify how the output changes with these operating conditions, and provides an instructive direction for improving the reactor performance. A key operating parameter to inspect in this study is the space velocity as it affects the CH_4 reaction time and the quantity of CH_4 that the reactor processes in unit time. Reactor pressure is another interesting parameter worth investigating, because increasing pressure can accelerate both forward reaction and reverse reaction of R1. Owning to the higher stoichiometric number of product gases in R1, higher pressure favors the reverse reaction. However, elevated pressure facilitates H_2 membrane permeation as well as CO_2 capture, hence it also favors forward reaction of R1 by removing more H_2 and CO_2. Fig. 15 predicated the performance of CH_4 conversion, H_2 generation rate and total H_2 yield within the initial 3 mins with varied space velocity and pressure. Increasing the space velocity led to declined CH_4 conversion due to the shortened

372 reaction time. But H_2 generation rate and H_2 total yield increased with space velocity
373 as the reactor processed more CH_4 per time. Higher pressure resulted in higher CH_4
374 conversion which indicated that the total effect of enhanced pressure is positive for
375 the forward reaction. The effect of pressure on the H_2 generation rate seems more
376 complicated. In the initial period of around 1 s, the H_2 generation rate is favored at
377 lower pressure, in agreement with the intrinsic nature of R1. But after 1 second, the
378 shift effect from the removal of H_2 and CO_2 started to dominate and higher pressure
379 provided more severe shift effect, as a result H_2 was produced at a faster rate at higher
380 pressures. The overall H_2 yield within 3 mins was enhanced gradually by elevated
381 pressure.

382 However, the advantage of SEMR only presented in limited period. With longer
383 time operation, the sorbents will reach to the saturation and thus the SEMR will
384 eventually become a simple MR. More capital cost is required to construct a SEMR
385 than a MR due to the addition of sorbents. But the sorbents only occupy the space and
386 become functionless when they are saturated. To reuse the sorbents, regeneration is
387 needed, as such the reactor has to be operated in batch system. The idea of sorption
388 enhancement for membrane reactor could be further improved by using moving bed
389 or circulating fluidized bed which could be operated in continuous system. Therefore,
390 the greater performance of SEMR over MR is sustained all the time. Another issue
391 associated with SEMR is the sorbent regeneration is general operated at high
392 temperature (>850 ºC) which makes the process energy intensive. Furthermore, the
393 possible interaction between catalyst and sorbent may affect the performance of

394 catalytic reaction and CO_2 capture. This issue is worth investigating in future studies.

395

396 5. Conclusions

397 A computational fluid dynamic (CFD) model, which allows the access of dynamic
398 and distributed information of reactants and products in a sorption-enhanced
399 membrane reactor, was developed in this study. The model was validated by
400 comparing the simulated results with experimental results obtained from a membrane
401 reactor without CO_2 sorbents. Further employment of this model was implemented to
402 explain the difference of reaction process between a SEMR and the traditional MR.
403 The results show that the SEMR not only reduced the CO_2 fraction, but also increased
404 the rates of MSR and WGS as well as the yield of H_2. The CO fraction level
405 decreased by 1 order of magnitude in the sorption-enhanced membrane reactor than
406 the traditional membrane reactor, which minimized the possibility of H_2 permeation
407 decay. With the detailed information inside a reactor which is blind to experimental
408 measurements, this model could be used as a general tool to analyze the reaction
409 process and interpret reactor performance.

410

411 **Nomenclature**

c	Gas concentration, mol m^{-3}
c_i	Gas concentration of component i, mol m^{-3}

D	Diffusion coefficient, $m^2\ s^{-1}$
DEN	Adsorption factor
$E_{k,MSR}$	Activation energy of rate coefficient for MSR, $J\ mol^{-1}$
$E_{K,MSR}$	Activation energy of equilibrium constant for MSR, $J\ mol^{-1}$
$E_{k,WGS}$	Activation energy of rate coefficient for WGS, $J\ mol^{-1}$
$E_{K,WGS}$	Activation energy of equilibrium constant for WGS, $J\ mol^{-1}$
J_{H_2}	H_2 permeation flux across membrane, $mol\ m^{-2}\ s^{-1}$
k_{MSR}	Rate coefficient of MSR, $mol\ Pa^{0.5}\ m^{-3}\ s^{-1}$
$k_{MSR,r}$	Rate coefficient of MSR at reference temperature, $mol\ Pa^{0.5}\ m^{-3}\ s^{-1}$
k_{WGS}	Rate coefficient of WGS, $mol\ Pa^{-1}\ m^{-3}\ s^{-1}$
$k_{WGS,r}$	Rate coefficient of WGS at reference temperature, $mol\ Pa^{-1}\ m^{-3}\ s^{-1}$
K_{CH_4}	Sorption coefficient for CH_4, Pa^{-1}
K_{CO}	Sorption coefficient for CO, Pa^{-1}
K_{H_2}	Sorption coefficient for H_2, Pa^{-1}
K_{H_2O}	Sorption coefficient for H_2O,
K_{MSR}	Equilibrium constant for MSR, Pa^2
$K_{MSR,r}$	Equilibrium constant for MSR at reference temperature, Pa^2
K_{WGS}	Equilibrium constant for WGS
$K_{WGS,r}$	Equilibrium constant for WGS at reference temperature
l	Space coordinate in membrane thickness direction, m
M_{max}	Maximum CO_2 molar capacity
p_{CH_4}	CH_4 partial pressure, Pa
p_{CO}	CO partial pressure, Pa
p_{CO_2}	CO_2 partial pressure, Pa

p_{H_2}	H_2 partial pressure, Pa
p_{H_2O}	H_2O partial pressure, Pa
Q	H_2 permeability through palladium membrane, mol m^{-1} s^{-1} $Pa^{-0.5}$
r	Radial coordinate, m
r_{CO_2}	CO_2 sorption rate, mol m^{-3} s^{-1}
r_{MSR}	MSR reaction rate, mol m^{-3} s^{-1}
r_{WGS}	WGS reaction rate, mol m^{-3} s^{-1}
R	Gas constant, 8.314 J mol^{-1} K^{-1}
S_{ct}	Source term for continuity equation
S_i	Source term for component balance equation
S_r	Source term in radial direction for Navier-Stokes equation
S_z	Source term in axial direction for Navier-Stokes equation
t	Time, s
T	Temperature, K
u_r	Radial velocity, m s^{-1}
u_θ	Tangential velocity, m s^{-1}
u_z	Axial velocity, m s^{-1}
z	Axial coordinate, m
α	Sorbent conversion
θ	Tangential coordinate
ρ	Density, kg m^{-3}
ρ_{mol}	Molar density of sorbent in the reactor, mol m^{-3}

412

413 **Abbreviations**

CFD	Computational fluid dynamics
MR	Membrane reactor
MSR	Methane steam reforming
PDE	Partial differential equation
SEMR	Sorption-enhanced membrane reactor
WGS	Water gas shift

414

415 Acknowledgement

416 M. Zhao thank for the support by the National Recruitment Program of Global Youth
417 Experts (The National Youth 1000 – Talent Program) of China (grant number:
418 20151710227) and the Tsinghua University Initiative Scientific Research Program
419 (grant number: 20161080094). G. Ji is grateful for the support by China Postdoctoral
420 Science Foundation (grant number: 2017M610910).

421

422 References

423 [1] R.C. Saxena, D. Seal, S. Kumar, H.B. Goyal. Thermo-chemical routes for
424 hydrogen rich gas from biomass: A review. Renew Sust Energ Rev 2008;12:1909-
425 1927.
426 [2] P. Ji, W. Feng, B. Chen. Production of ultrapure hydrogen from biomass
427 gasification with air. Chem Eng Sci 2009;64:582-592.
428 [3] R. Khonde, A. Chaurasia. Rice husk gasification in a two-stage fixed-bed gasifier:
429 Production of hydrogen rich syngas and kinetics. Int J Hydrogen Energy
430 2016;41:8793-8802.
431 [4] S.H.D. Lee, D.V. Applegate, S. Ahmed, S.G. Calderone, T.L. Harvey. Hydrogen
432 from natural gas: part I—autothermal reforming in an integrated fuel processor. Int J
433 Hydrogen Energy 2005;30:829-842.

[5] J.R.H. Ross. Natural gas reforming and CO_2 mitigation. Catal Today 2005;100:151-158.
[6] H. Jin, Y. Lu, B. Liao, L. Guo, X. Zhang. Hydrogen production by coal gasification in supercritical water with a fluidized bed reactor. Int J Hydrogen Energy 2010;35:7151-7160.
[7] G.J. Stiegel, M. Ramezan. Hydrogen from coal gasification: An economical pathway to a sustainable energy future. Int J Coal Geol 2006;65:173-190.
[8] T.C. Woodbridge, D.D. Woodbridge. Ocean hydrogen for launch operations. Int J Hydrogen Energy 1996;21:81-86.
[9] J. Martinez-Frias, A.-Q. Pham, S. M. Aceves. A natural gas-assisted steam electrolyzer for high-efficiency production of hydrogen. Int J Hydrogen Energy 2003;28:483-490.
[10] B. McLellan, E. Shoko, A.L. Dicks, J.C. Diniz da Costa. Hydrogen production and utilisation opportunities for Australia. Int J Hydrogen Energy 2005;30:669-679.
[11] J. Adanez, A. Abad, F. Garcia-Labiano, P. Gayan, L.F. de Diego. Progress in chemical-looping combustion and reforming technologies. Prog Energy Combust Sci 2012;38:215-282.
[12] E. Fernandez, K. Coenen, A. Helmi, J. Melendez, J. Zuñiga, D.A. Pacheco Tanaka, M. van Sint Annaland, F. Gallucci. Preparation and characterization of thin-film Pd–Ag supported membranes for high-temperature applications. Int J Hydrogen Energy 2015;40:13463-13478.
[13] S. Yun, S. Ted Oyama. Correlations in palladium membranes for hydrogen separation: A review. J Membrane Sci 2011;375:28-45.
[14] B. Ballinger, J. Motuzas, S. Smart, J.C. Diniz da Costa. Palladium cobalt binary doping of molecular sieving silica membranes. Journal of Membrane Science 2014;451:185-191.
[15] G. Ji, S. Smart, S.K. Bhatia, J.C. Diniz da Costa. Improved pore connectivity by the reduction of cobalt oxide silica membranes. Sep Purif Technol 2015;154:338-344.
[16] M. Patrascu, M. Sheintuch. On-site pure hydrogen production by methane steam reforming in high flux membrane reactor: Experimental validation, model predictions and membrane inhibition. Chem Eng J 2015;262:862-874.
[17] J. Tong, Y. Matsumura. Effect of catalytic activity on methane steam reforming in hydrogen-permeable membrane reactor. Appl Catal A-Gen 2005;286:226-231.
[18] W.-H. Chen, T.-C. Hsieh, T.L. Jiang. An experimental study on carbon monoxide conversion and hydrogen generation from water gas shift reaction. Energy Convers Manage 2008;49:2801-2808.
[19] S. Battersby, S. Smart, B. Ladewig, S. Liu, M.C. Duke, V. Rudolph, J.C.D.d. Costa. Hydrothermal stability of cobalt silica membranes in a water gas shift membrane reactor. Sep Purif Technol 2009;66:299-305.
[20] S. Battersby, P.W. Teixeira, J. Beltramini, M.C. Duke, V. Rudolph, J.C. Diniz da Costa. An analysis of the Peclet and Damkohler numbers for dehydrogenation reactions using molecular sieve silica (MSS) membrane reactors. Catal Today 2006;116:12-17.
[21] B. Anzelmo, J. Wilcox, S. Liguori. Natural gas steam reforming reaction at low

temperature and pressure conditions for hydrogen production via Pd/PSS membrane reactor. J Membrane Sci 2017;522:343-350.
[22] J. Boon, J.A.Z. Pieterse, F.P.F. van Berkel, Y.C. van Delft, M. van Sint Annaland. Hydrogen permeation through palladium membranes and inhibition by carbon monoxide, carbon dioxide, and steam. J Membrane Sci 2015;496:344-358.
[23] W.-H. Chen, P.-C. Hsu. Hydrogen permeation measurements of Pd and Pd–Cu membranes using dynamic pressure difference method. Int J Hydrogen Energy 2011;36:9355-9366.
[24] M. Coroneo, G. Montante, J. Catalano, A. Paglianti. Modelling the effect of operating conditions on hydrodynamics and mass transfer in a Pd–Ag membrane module for H_2 purification. J Membrane Sci 2009;343:34-41.
[25] J. Tong, Y. Matsumura, H. Suda, K. Haraya. Experimental study of steam reforming of methane in a thin (6 μm) pd-based membrane reactor. Ind Eng Chem Res 2005;44:1454-1465.
[26] S. Battersby, M.C. Duke, S. Liu, V. Rudolph, J.C.D.d. Costa. Metal doped silica membrane reactor: Operational effects of reaction and permeation for the water gas shift reaction. J Membrane Sci 2008;316:46-52.
[27] M. Shokrollahi Yancheshmeh, H.R. Radfarnia, M.C. Iliuta. High temperature CO_2 sorbents and their application for hydrogen production by sorption enhanced steam reforming process. Chem Eng J 2016;283:420-444.
[28] M. Zhao, X. Yang, T.L. Church, A.T. Harris. Interaction between a bimetallic Ni–Co catalyst and micrometer-sized CaO for enhanced H_2 production during cellulose decomposition. Int J Hydrogen Energy 2011;36:421-431.
[29] L. Barelli, G. Bidini, F. Gallorini, S. Servili. Hydrogen production through sorption-enhanced steam methane reforming and membrane technology: A review. Energy 2008;33:554-570.
[30] E. Ochoa-Fernández, C. Lacalle-Vilà, T. Zhao, M. Rønning, D. Chen, Experimental demonstration of H_2 production by CO_2 sorption enhanced steam methane reforming using ceramic acceptors, in: M.S. Fábio Bellot Noronha, S.-A. Eduardo Falabella (Eds.) Studies in Surface Science and Catalysis, Elsevier, 2007, pp. 159-164.
[31] E. Ochoa-Fernandez, G. Haugen, T. Zhao, M. Ronning, I. Aartun, B. Borresen, E. Rytter, M. Ronnekleiv, D. Chen. Process design simulation of H_2 production by sorption enhanced steam methane reforming: evaluation of potential CO_2 acceptors. Green Chemistry 2007;9:654-662.
[32] E.R. van Selow, P.D. Cobden, P.A. Verbraeken, J.R. Hufton, R.W. van den Brink. Carbon capture by sorption-enhanced water−gas shift reaction process using hydrotalcite-based material. Ind Eng Chem Res 2009;48:4184-4193.
[33] F.R. García-García, M. León, S. Ordóñez, K. Li. Studies on water–gas-shift enhanced by adsorption and membrane permeation. Catal Today 2014;236, Part A:57-63.
[34] M.A. Soria, S. Tosti, A. Mendes, L.M. Madeira. Enhancing the low temperature water–gas shift reaction through a hybrid sorption-enhanced membrane reactor for high-purity hydrogen production. Fuel 2015;159:854-863.

[35] Y. Chen, A. Mahechabotero, C.J. Lim, J.R. Grace, J. Zhang, Y. Zhao, C. Zheng. Hydrogen production in a sorption-enhanced fluidized-bed membrane reactor: operating parameter investigation. Ind Eng Chem Res 2014;53:6230-6242.

[36] Z. Chen, F. Po, J.R. Grace, C. Jim Lim, S. Elnashaie, A. Mahecha-Botero, M. Rakib, Y. Shirasaki, I. Yasuda. Sorbent-enhanced/membrane-assisted steam-methane reforming. Chem Eng Sci 2008;63:170-182.

[37] M.K. Koukou, N. Papayannakos, N.C. Markatos. On the importance of non-ideal flow effects in the operation of industrial-scale adiabatic membrane reactors. Chem Eng J 2001;83:95-105.

[38] G. Ji, G. Wang, K. Hooman, S. Bhatia, J. Diniz da Costa. Computational fluid dynamics applied to high temperature hydrogen separation membranes. Front Chem Sci Eng 2012;6:3-12.

[39] J. Xu, G.F. Froment. Methane steam reforming, methanation and water-gas shift: I. Intrinsic kinetics. AlChE J 1989;35:88-96.

[40] K. Hou, R. Hughes. The kinetics of methane steam reforming over a Ni/α-Al_2O catalyst. Chem Eng J 2001;82:311-328.

[41] A. Iulianelli, S. Liguori, J. Wilcox, A. Basile. Advances on methane steam reforming to produce hydrogen through membrane reactors technology: A review. Catal Rev 2016;58:1-35.

[42] J. Xu, G.F. Froment. Methane steam reforming: II. Diffusional limitations and reactor simulation. AlChE J 1989;35:97-103.

[43] G.L. Holleck. Diffusion and solubility of hydrogen in palladium and palladium--silver alloys. J Phys Chem 2002;74.

[44] T.L. Ward, T. Dao. Model of hydrogen permeation behavior in palladium membranes. J Membrane Sci 1999;153:211-231.

[45] H.R. Radfarnia, M.C. Iliuta. Application of surfactant-template technique for preparation of sodium zirconate as high temperature CO_2 sorbent. Sep Purif Technol 2012;93:98-106.

[46] T. Zhao, E. Ochoa-Fernández, M. Rønning, D. Chen. Preparation and high-temperature CO_2 capture properties of nanocrystalline Na_2ZrO_3. Chem Mater 2007;19:3294-3301.

[47] I. Alcérreca-Corte, E. Fregoso-Israel, H. Pfeiffer. CO_2 absorption on Na_2ZrO_3: A kinetic analysis of the chemisorption and diffusion processes. J Phys Chem C 2008;112:6520-6525.

[48] L. Martínez-dlCruz, H. Pfeiffer. Cyclic CO_2 chemisorption–desorption behavior of Na_2ZrO_3: Structural, microstructural and kinetic variations produced as a function of temperature. J Solid State Chem 2013;204:298-304.

[49] T. Zhao, M. Rønning, D. Chen. Preparation of nanocrystalline Na_2ZrO_3 for high-temperature CO_2 acceptors: chemistry and mechanism. J Energy Chem 2013;22:387-393.

[50] L. Martínez-dlCruz, H. Pfeiffer. Microstructural thermal evolution of the Na_2CO_3 phase produced during a Na_2ZrO_3–CO_2 chemisorption process. J Phys Chem C 2012;116:9675-9680.

[51] G.G. Santillán-Reyes, H. Pfeiffer. Analysis of the CO_2 capture in sodium

566 zirconate (Na_2ZrO_3). Effect of the water vapor addition. Int J Green Gas Con
567 2011;5:1624-1629.
568 [52] M.Z. Memon, X. Zhao, V.S. Sikarwar, A.K. Vuppaladadiyam, S.J. Milne, A.P.
569 Brown, J. Li, M. Zhao. Alkali metal CO_2 sorbents and the resulting metal carbonates:
570 potential for process intensification of sorption-enhanced steam reforming. Environ
571 Sci Technol 2017;51:12-27.
572 [53] D. Sutton, B. Kelleher, J.R.H. Ross. Review of literature on catalysts for biomass
573 gasification. Fuel Process Technol 2001;73:155-173.
574 [54] J. Tong, Y. Matsumura. Pure hydrogen production by methane steam reforming
575 with hydrogen-permeable membrane reactor. Catal Today 2006;111:147-152.
576

578 # Table

579 **Table 1.** Boundary conditions of the CFD model

Parameters	Value	Parameters	Value
Membrane diameter (m)	9.5×10^{-3}	**H_2 permeance (mol m^{-2} s^{-1} $Pa^{-0.5}$)**	Membrane_L: 9.38×10^{-4}
Reactor diameter (m)	1.7×10^{-2}		Membrane_H: 1.88×10^{-3}
Membrane length (m)	7.0×10^{-2}	**Space velocity (h^{-1})**	1120 (Re≈2.8)
Temperature	500 ℃		2240 (Re≈5.6)
CH_4/H_2O molar ratio	1/3		3360 (Re≈8.4)
Outlet pressure (MPa)	0.3	**Turbulence**	Laminar

Figures

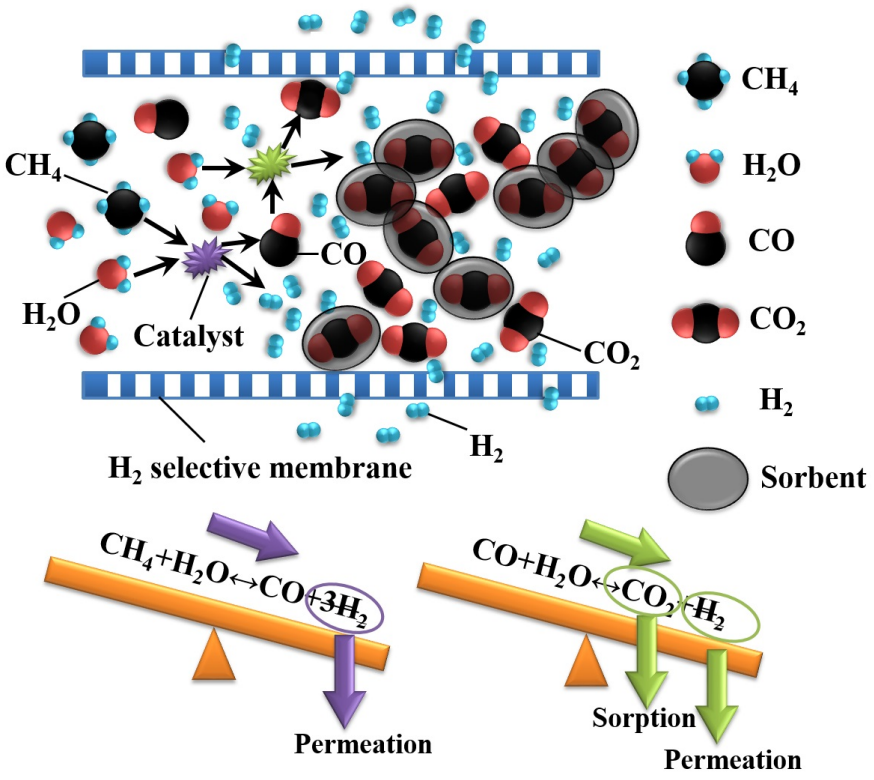

Fig. 1 The schematic of methane steam reforming in a membrane reactor with *in-situ* CO_2 capture.

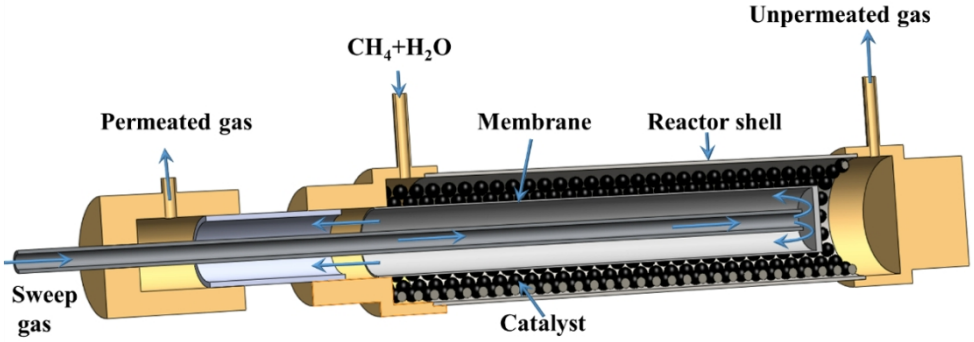

Fig. 2 The structure of a membrane reactor for methane steam reforming.

588

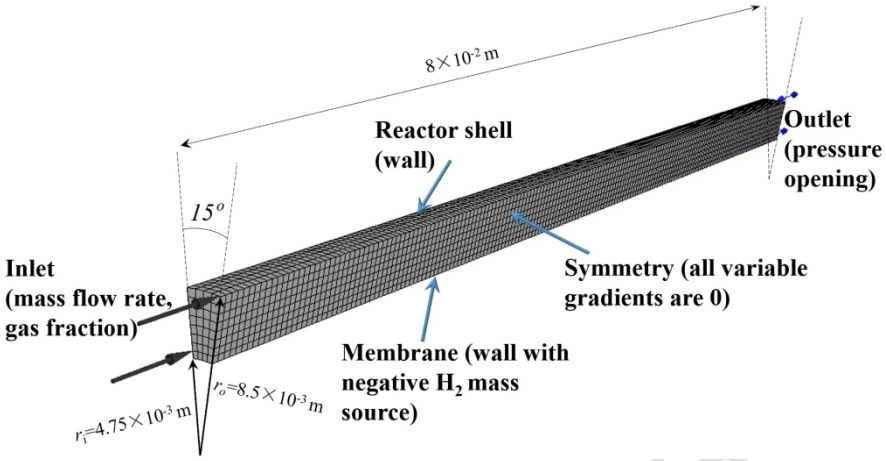

589

590 **Fig. 3** The reaction domain and boundary conditions in CFD model.

591

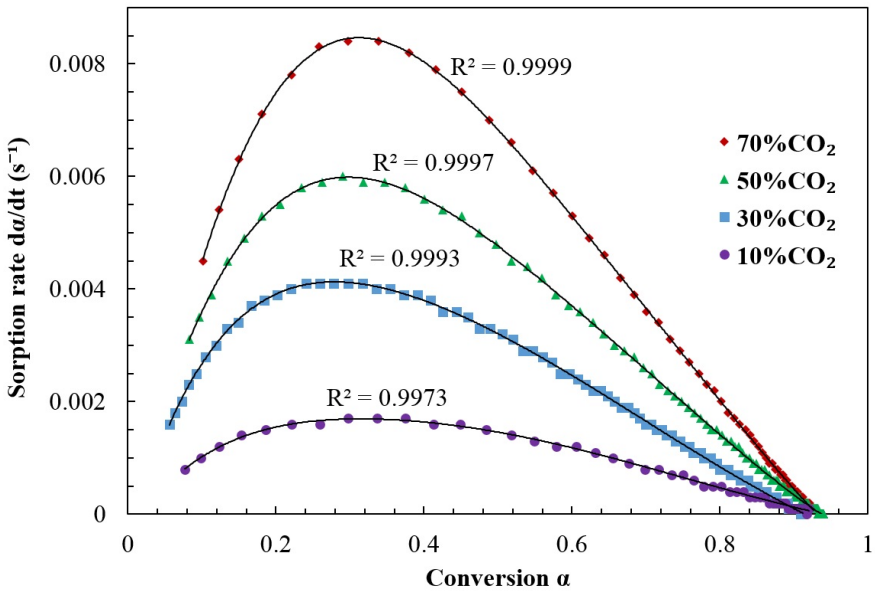

592

593 **Fig. 4** CO_2 sorption kinetics in Na_2ZrO_3 under various CO_2 partial pressures with

594 CO_2-N_2 mixture at 500 ºC. (●)10 vol.% of CO_2 in N_2; (■) 30 vol.% of CO_2 in N_2; (▲)

595 50 vol.% of CO_2 in N_2; (◆) 70 vol.% of CO_2 in N_2;

596

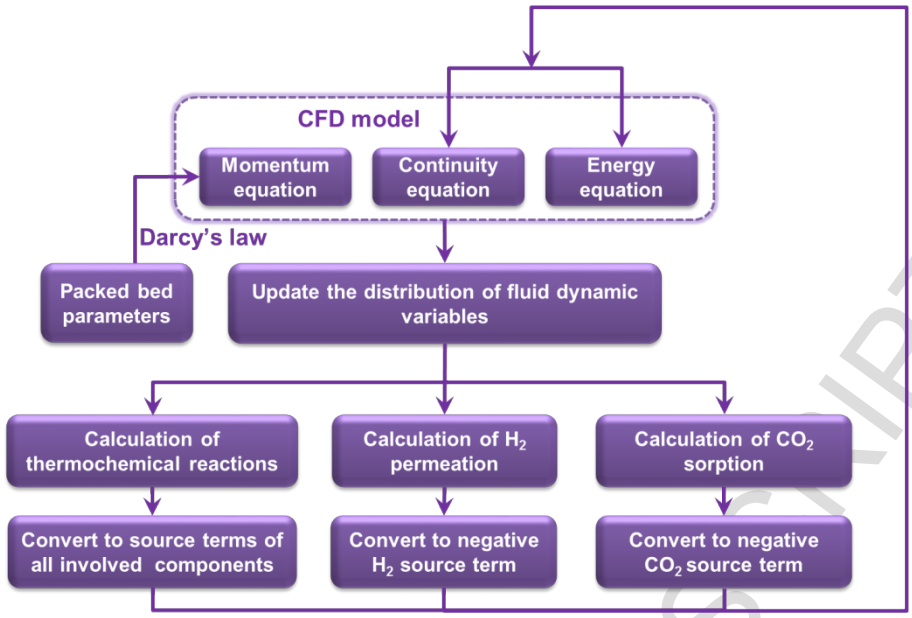

Fig. 5 The Program flow chart of CFD model

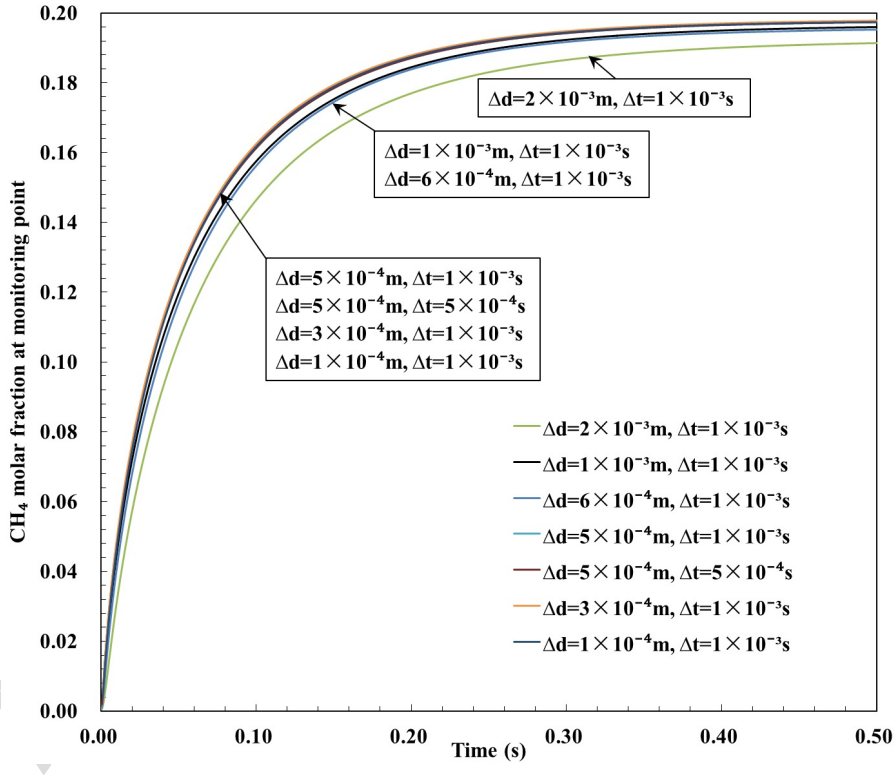

Fig. 6 The comparison of monitored CH_4 mass fraction in varying mesh and time-step combinations (Monitored location is 1cm away from inlet).

603

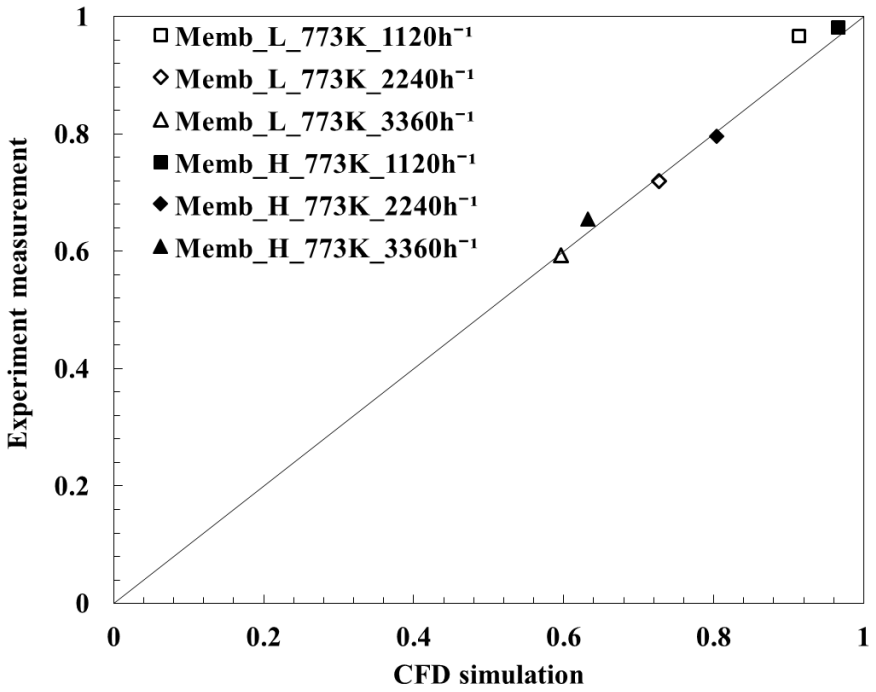

604

605 **Fig. 7** The comparison of CH_4 conversion resulted from experiment and CFD model.

606 (□) Low performance membrane at 773 K with space velocity 1120 h^{-1}; (◇) Low performance

607 membrane at 773 K with space velocity 2240 h^{-1}; (△) Low performance membrane at 773 K with

608 space velocity 3360 h^{-1}; (■) High performance membrane at 773 K with space velocity 1120 h^{-1};

609 (◆) High performance membrane at 773 K with space velocity 2240 h^{-1}; (▲) High performance

610 membrane at 773 K with space velocity 3360 h^{-1}; Experimental data was reproduced from [54]

611

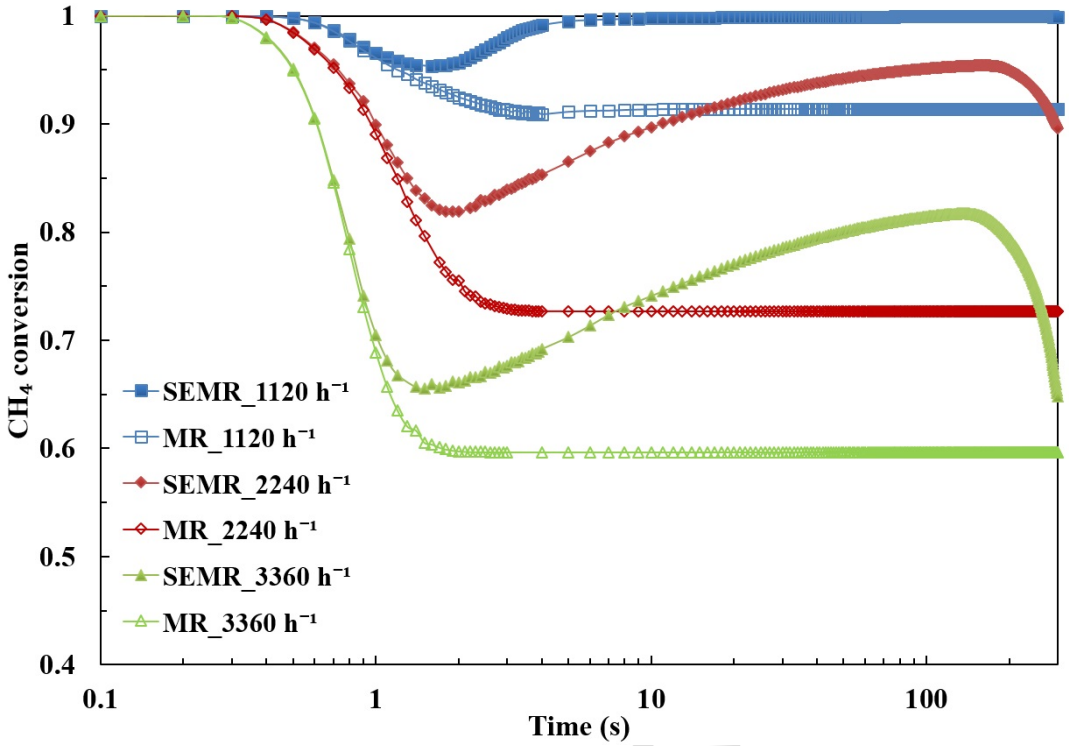

612

613 **Fig. 8** CH_4 conversion of membrane reactor and sorption enhanced membrane reactor

614 under different space velocities. (■) Sorption enhanced membrane reactor under 1120 h^{-1}; (⊟)

615 Simple membrane reactor under 1120 h^{-1}; (◆) Sorption enhanced membrane reactor under 2240 h^{-1};

616 (◇) Simple membrane reactor under 2240 h^{-1}; (▲) Sorption enhanced membrane reactor under

617 3360 h^{-1}; (△) Simple membrane reactor under 3360 h^{-1}.

618

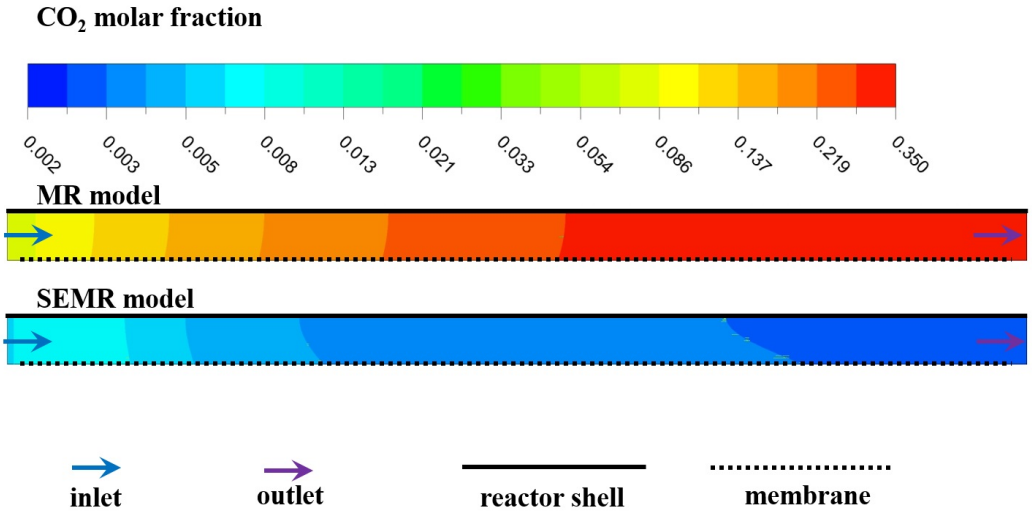

619

620 **Fig. 9** The distribution of CO_2 molar fraction in membrane reactor and sorption-

621 enhanced membrane reactor at the 100th sec.

622

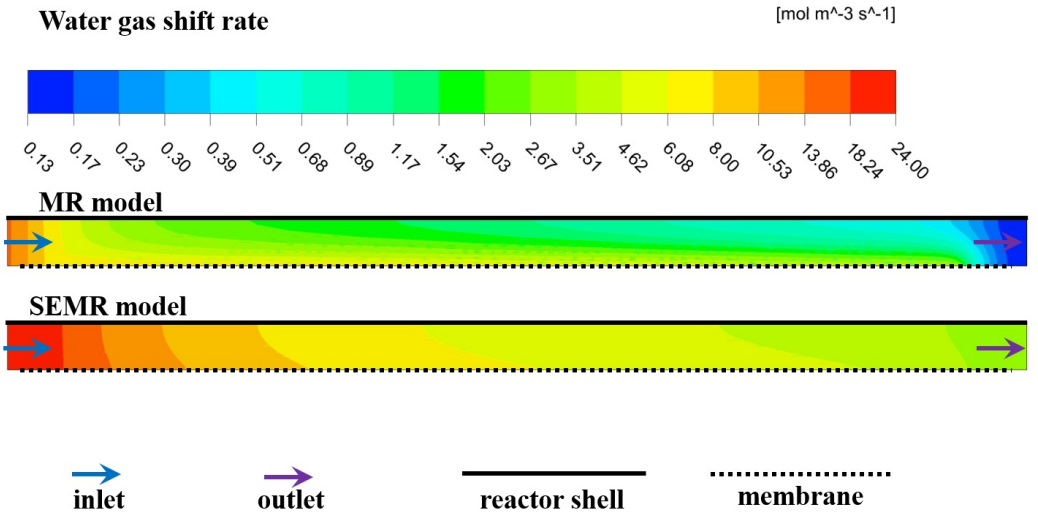

623

624 **Fig. 10** The distribution of water gas shift reaction rate in membrane reactor and

625 sorption enhanced membrane reactor at the 100th sec.

626

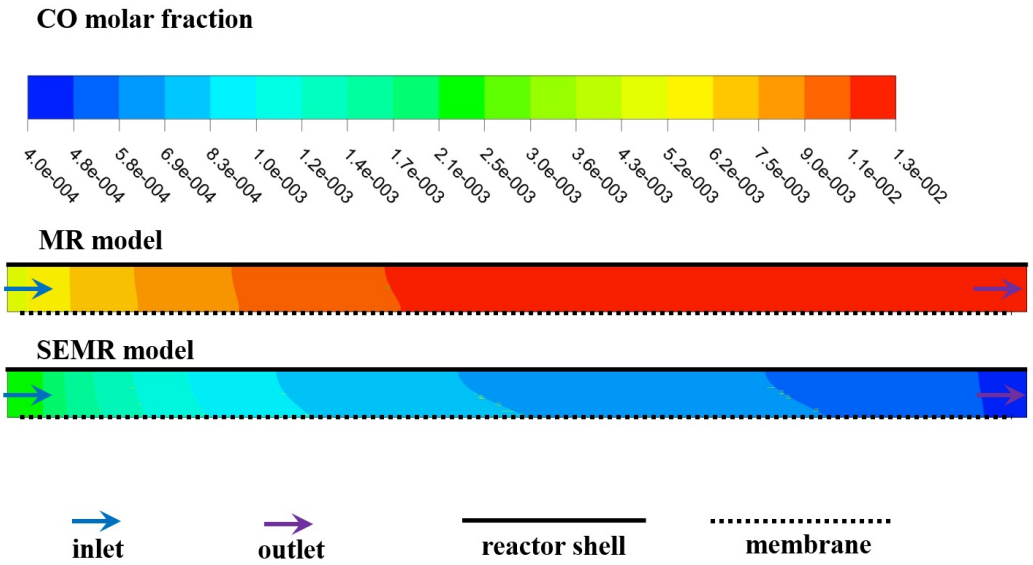

627

628 **Fig. 11** The distribution of CO molar fraction in membrane reactor and sorption

629 enhanced membrane reactor at the 100th sec.

630

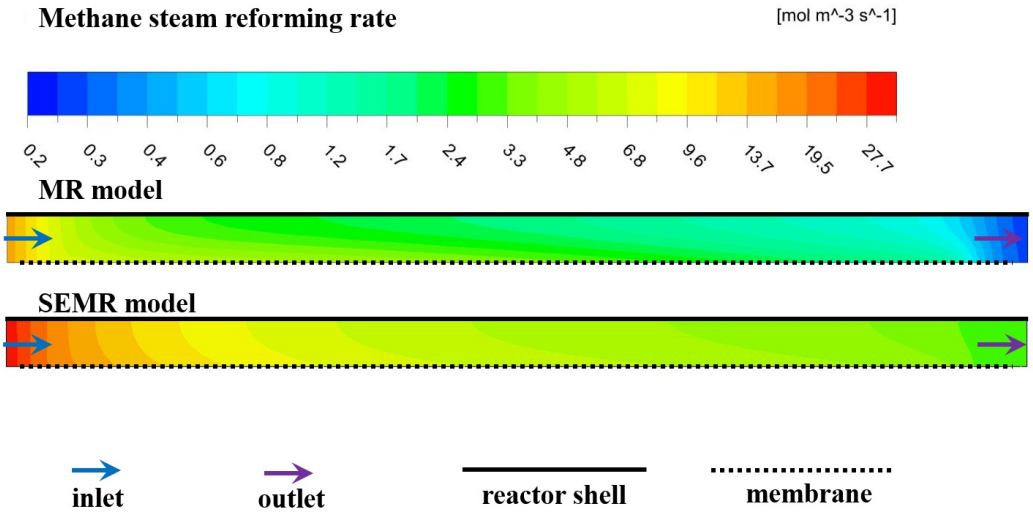

631

632 **Fig. 12** The distribution of methane steam reforming rate in membrane reactor and

633 sorption enhanced membrane reactor at the 100th sec.

634

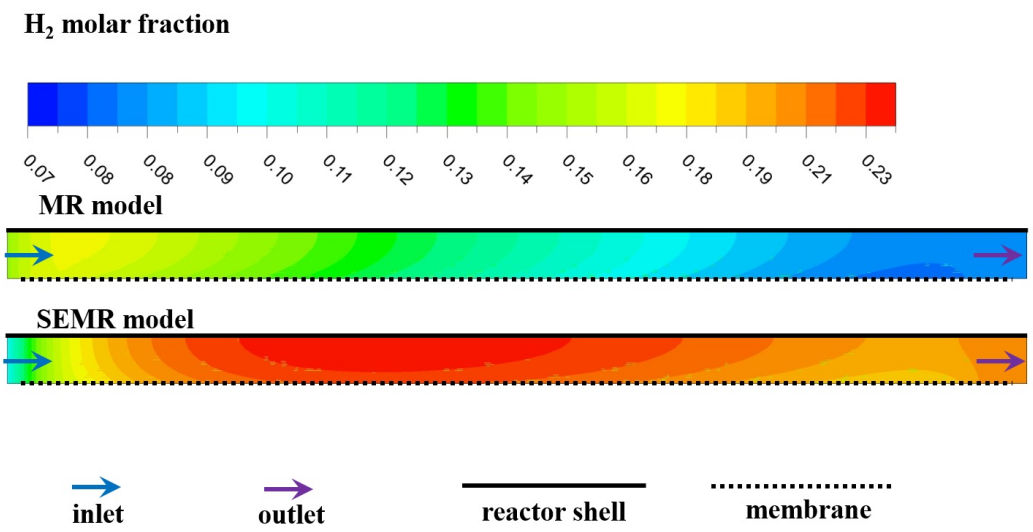

635

636 **Fig. 13** The distribution of H_2 molar fraction in membrane reactor and sorption

637 enhanced membrane reactor at the 100th sec.

638

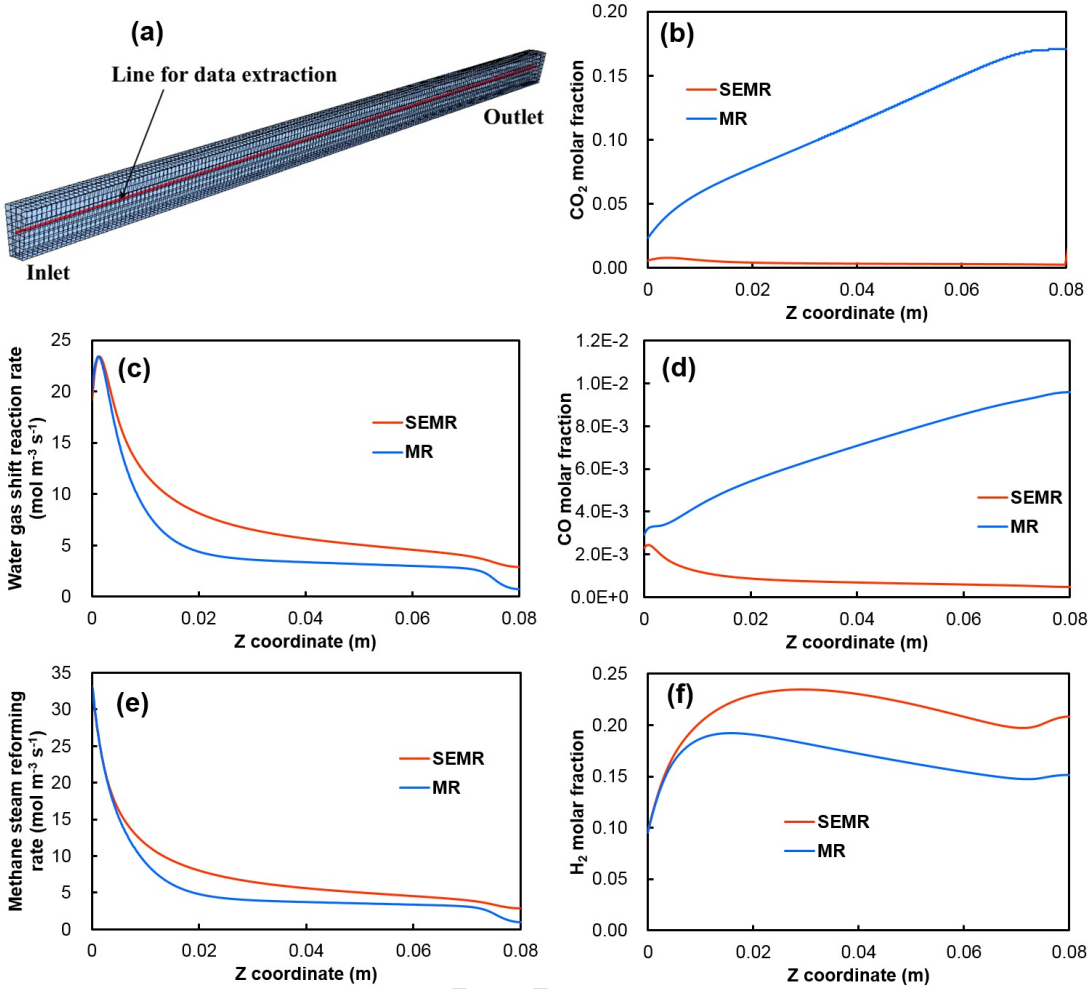

Fig. 14. The variations of CO_2 fraction, WGS rate, CO fraction, MSR rate and H_2 fraction along a line from inlet to outlet. (a) the location of the line to extract these variables, from (6.625×10^{-3} m, 0 rad, 0 m) to (6.625×10^{-3} m, 0 rad, 8×10^{-2} m) in cylindrical coordinate; (b) CO_2 molar fraction; (c) water gas shift reaction rate; (d) CO molar fraction; (e) methane steam reforming reaction rate; (f) H_2 molar fraction.

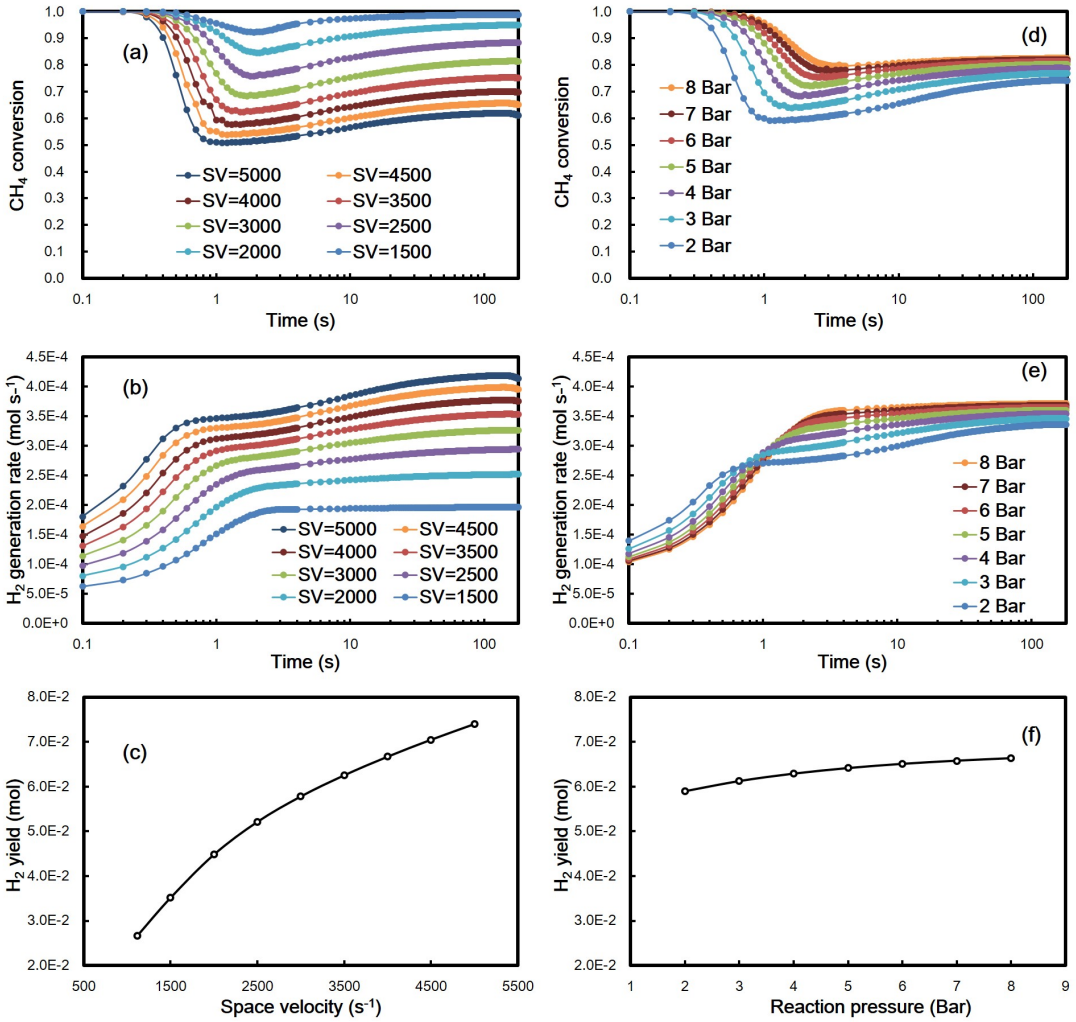

645

646 **Fig. 15** Predicted performance of SEMR at different conditions. (a) CH_4 conversion at different

647 space velocities (*S/C*=3; *P*=3 Bar); (b) H_2 generation rate at different space velocities (*S/C*=3; *P*=3

648 Bar); (c) H_2 yield within 3 mins at different space velocities (*S/C*=3; *P*=3 Bar); (d) CH_4

649 conversion at different pressures (*S/C*=3; *SV*=3360 s^{-1}); (e) H_2 generation rate at different

650 pressures (*S/C*=3; *SV*=3360 s^{-1}) and (f) H_2 yield within 3 mins at different pressures (*S/C*=3;

651 *SV*=3360 s^{-1}).

Highlights

- Sorption enhanced membrane reactor was proposed to enhance H_2 yield.
- H_2 permeation and CO_2 capture interacted with methane steam reforming.
- Validated CFD model assessed the enhancements of methane steam reforming.
- Na_2ZrO_3 sorbents significantly increased the H_2 yield and CH_4 conversion.
- CO poisoning to palladium membrane was also minimized by CO_2 removal.